Near Surface Geophysics, 2014, **12**, 165-178 doi: 10.3997/1873-0604.2013052

Joint interpretation of geoelectrical and soil-gas measurements for monitoring CO_2 releases at a natural analogue

U. Sauer*, N. Watanabe, A. Singh, P. Dietrich, O. Kolditz and C. Schütze

UFZ – Helmholtz Centre for Environmental Research, Department Monitoring and Exploration Technologies, Permoserstrasse 15, 04318 Leipzig, Germany

Received May 2012, revision accepted September 2013

ABSTRACT

The development and validation of hierarchic monitoring concepts is essential for detecting and assessing possible leakages from storage formations, especially for carbon capture and storage (CCS) applications. Joint interpretation of various techniques (such as carbon dioxide (CO_2) concentration and flux measurements, self-potential (SP) and geoelectrical surveys) showed that the combination of geophysical methods with soil-gas analysis for mesoscale monitoring of the shallow subsurface above geologic CO_2 storages can be a valuable tool for mapping and monitoring potential CO_2 spread in the subsurface. Three measurement campaigns were undertaken – May 2011, July 2011 and April 2012 – at an analogue site in the Cheb Basin, Czech Republic, with the aim of studying CO_2 leakages and their temporal and spatial behaviour. Results of geoelectrical investigations give an insight into the structural features of the subsurface. CO_2 discharge into the atmosphere is mostly impeded by shallow, clay-rich, partly water-saturated zones, which can be seen in the electrical resistivity tomography (ERT) results. Several transport processes can be identified based on SP measurements. The SP results highlight the complex behaviour of temporal variations for the flow patterns. In particular, coupled migration of gas and water plays an important influencing role in this process. Site-specific, near surface geological features and meteorological conditions seem to exert great influence on the degassing pattern and measured CO_2 values. Therefore, soil-gas measurements represent a snapshot which illustrates both a distinct typical pattern of the soil-gas distribution in the near subsurface and certain differences caused by soil and meteorological conditions. Observed CO_2 soil-gas anomalies and modelled results suggest that the occurrence of gas discharge is much more localized around restricted areas, often controlled by local permeability contrasts. Hence, our results show that a proposed monitoring concept should integrate SP, time-lapse ERT, meteorological parameters and soil-gas measurements to provide a comprehensive insight into the subsurface structures and processes.

INTRODUCTION

In recent years, global concerns about greenhouse gas emissions have stimulated considerable interest in carbon capture and storage (CCS) as a potential 'bridging technology' that can achieve significant carbon dioxide (CO_2) emission reductions, while simultaneously allowing fossil fuels to be used until alternative energy sources are more widely available and deployed (McCoy and Rubin 2005). Preliminary estimates, carried out with a view to assessing the impact of the EU Directive on geological CO_2 storage and referred to in the impact assessment of the Commission, indicate that 7 million tonnes of CO_2 could be stored by 2020, and up to 160 million tonnes by 2030, equating to a 20% reduction in greenhouse gas emissions by 2020, which could help achieve the stated goal of a 30% reduction of CO_2 in the developed world by this date (European Parliament and the Council 2009).

In the last few years, there have been several research and development projects on CCS, and some governments have begun to commercially introduce CCS methods into practice. The storage of CO_2 in saline aquifers is seen as the option with the most potential to achieve substantial CO_2 reductions at acceptable cost levels over the next few decades (Norden 2011). However, there are still uncertainties related to the large-scale implementation of this emergent technology, while public perception of CO_2 storage in the geosphere remains generally negative, motivated in particular by perceived leakage risks. Already as early as 2004, Itaoka, Saito and Akai (2004) identified and summarized four important factors that influence public opinion of this technology. These concerns relate to uncertainty over the environmental impacts and risks caused by CO_2 injection (including possibility of leakage), the effectiveness of CCS and its potential as a useful mitigation option that takes climate change into account, factors relating to societal responsibility for the

* uta.sauer@ufz.de

environment, and lastly the dependence of CCS on continued fossil fuel use. The EU Directive on the geological storage of CO_2 (known as the 'CCS Directive') established a legal framework for environmentally safe geological storage of CO_2, and defined minimum conditions for closure of CCS facilities, such as a responsibility to ensure that the actual behaviour of the injected CO_2 conforms with modelled behaviour, that no detectable leakages are present, and that the storage site is evolving towards a situation of long-term stability. Successful monitoring depends on the instruments utilized, and requires the identification of appropriate methods to provide the required information about potential leakages in real time. Therefore, the main issues for future large-scale industrial application and for broad public acceptance of CCS technology are the development and validation of monitoring technologies, and the availability of an integrated risk assessment strategy (Schütze *et al.* 2012b).

Within the framework of the MONACO project (MONACO = Monitoring approach for geological CO_2 storage sites using a hierarchic observation concept, funded by the German Priority Program GEOTECHNOLOGIEN, started in September 2011) an integrative hierarchic monitoring concept is proposed to reliably detect and assess possible leakages from storage formations into the shallow subsurface (including aquifers and the unsaturated zone) and degassing of CO_2 into the atmosphere (Sauer *et al*. 2013). To enable monitoring of large-scale sites for potential CO_2 leakages, several methods will be either combined or used complementarily to one another and applied at different scales, such as open-path Fourier transform infrared (OP-FTIR) spectrometry, soil-gas analytics, geophysics and direct-push technology, and results will subsequently be jointly interpreted. Within this project, naturally occurring CO_2 deposits provide unique natural analogues for evaluating and validating methods used for the detection and monitoring of CO_2 spread and potential degassing into the atmosphere, while simultaneously facilitating the gathering of valuable information (e.g., Holloway *et al.* 2007; Lewicki *et al.* 2007; Battani *et al.* 2010; Gal *et al.* 2011; Schütze *et al.* 2012b). This information helps broaden knowledge concerning the chemical and physical processes taking place.

A large amount of subsurface effects related to naturally occurring CO_2 can be used to help us further understand processes which have to be considered when developing a reliable health, safety and environmental risk assessment strategy (Schütze *et al.* 2012b). In this paper we show how a joint application of geophysical methods in combination with soil-gas measurements can be used for the detection of CO_2 degassing areas and what kind of constraints exist.

NATURAL ANALOGUE TEST SITE

The Cheb Basin (NW Bohemia, Czech Republic) is an example of such a natural analogue where CO_2 leakage occurs. It offers a perfect location to verify and validate monitoring tools for the direct investigation of processes along preferential migration paths (Fig. 1). The geological and hydrological structures of the Cheb Basin are manifested by episodic Cenozoic volcanism (the youngest at 0.2–0.5 Ma), repeated earthquake swarms, numerous mineral springs, CO_2 emissions with high ^3He content, and CO_2-rich mineral springs and natural gas seeps (known as mofettes). Several active tectonic faults and deep processes are responsible for the occurrence of CO_2 in the Cheb Basin, and the gas (up to 99.99% CO_2) ascends via tectonic fault zones directly from the upper mantle to the surface (Bräuer *et al.* 2008, 2011). The existing mofettes along the Mariánské Lázně fault (MLF) and the Počatky-Plesná fault zone (PPZ) are an indication of preferential CO_2 migration pathways. This area features the presence of both focused small-scale CO_2 degassing sites (such as the CO_2-rich

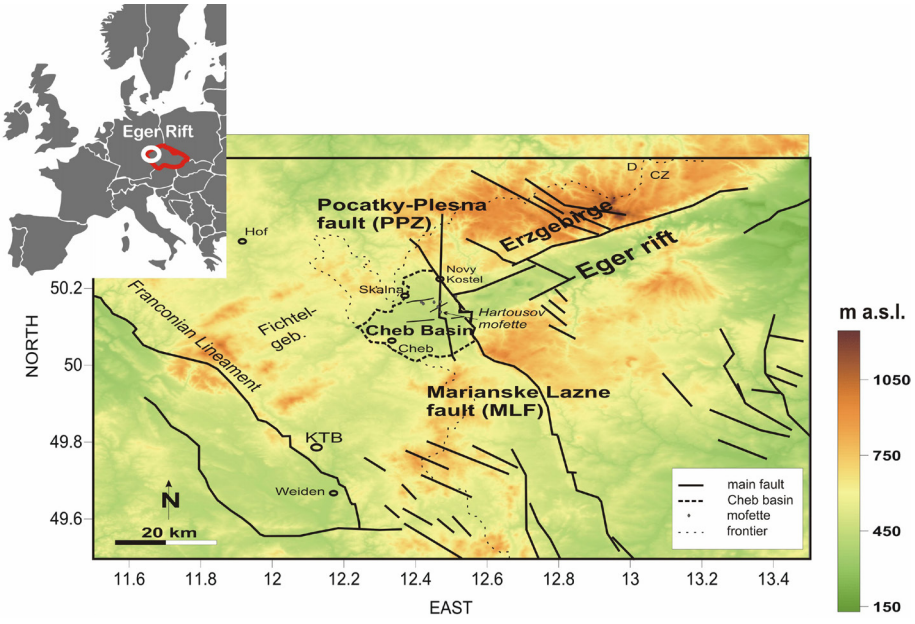

FIGURE 1
The border region Vogtland/NW Bohemia is one of the most tectonically active regions in Central Europe. The Cheb Basin is situated in the western Eger rift. The most important deep-reaching N-S trending faults involving the Cheb Basin are the Mariánské Lázně fault (MLF) and the Počatky-Plesná fault zone (PPZ) (after Bankwitz *et al.* 2003). The elevation map is derived from STRM 90 m Digital Elevation Data Base (Jarvis *et al.* 2008). The CO_2-rich mineral springs and natural gas seeps (known as mofettes) along the PPZ and MLF are an indication of preferential CO_2 migration pathways.

mineral springs) and mofettes along the major faults, and larger areas with diffuse degassing behaviour characterized by stressed vegetation (Kämpf *et al.* 2012).

METHODS AND DATA ACQUISITION

Natural leakages of CO_2 from geological reservoirs can be found at various volcanic, hydrothermal and tectonically active regions. With this in mind, it has been shown that the use of soil-gas measurement techniques and geophysical methods are useful for the identification of such leakages (e.g., Chiodini *et al.* 1998; Annunziatellis *et al.* 2008; Byrdina *et al.* 2009; Carapezza *et al.* 2009; Finizola *et al.* 2009; Pettinelli *et al.* 2010; Revil *et al.* 2011). Soil-gas emanation surveys represent a geochemical approach for the delineation of fault zones. The determination of soil-gas flux rates can be used to quantify release rates and hence be used for the characterization of migration process dynamics. This method allows reliable values of soil CO_2 degassing rates to be obtained, e.g. from environmental research undertaken, in geothermal and volcanic areas (Chiodini *et al.* 1998, 2008; Lewicki 2003; Carapezza *et al.* 2009; Johansson *et al*. 2011). In these surveys, soil gas is typically sampled at the surface or in shallow soil depths (Chiodini *et al.* 1998; Ciotoli *et al.* 1999; Yang *et al.* 2003, 2005; Etiope and Lombardi 1995; Etiope *et al*. 2005; Walia *et al.* 2010). Soil-gas concentration and flux measurement techniques are relatively simple to perform and are valuable methods for the monitoring of seeping CO_2 along preferential pathways (e.g., Voltattorni *et al.* 2009; Bennati *et al.* 2011). Long-term soil-gas measurements at undisturbed locations often show a strong correlation between soil-gas concentration or fluxes and soil moisture conditions, as well as links to the meteorological situation. Therefore, it should be noted that the analysis of soil-gas concentration and flux data without taking influencing parameters into account can lead to misinterpretation.

The application of geophysical methods is motivated by two main processes which should be considered. Firstly, gaseous CO_2 intrusion into shallow groundwater systems generally causes increased gas phase content in the soil pore space, which accordingly leads to increased bulk resistivity. However, subsequent dissolution of CO_2 in sediments that have been partially saturated with groundwater leads to the occurrence of carbonic acid, followed by generally decreased pH values and increased alkalinity (Kharaka *et al.* 2010; Börner *et al.* 2012; Lamert *et al.* 2012). In this environment, ions are being mobilized; leading to a higher electrical conductivity or lower resistivity, respectively. This impact on electrical resistivity could be measured using electrical resistivity tomography (ERT) and electromagnetic induction (EMI) methods (Rein, Hoffmann and Dietrich 2004; Lamert *et al.* 2012). Information on the distribution of resistivity can be applied to map shallow subsurface structures depending on the depth of investigation, which is subject to electrode spacing, the electrode configuration and the resistivity distribution of the subsurface (e.g., Hoffmann and Dietrich 2004). In this context, the determination of resistivity anomalies is considered to be useful when investigating disturbances caused by variations in lithological parameters and fluid content (Wannamaker *et al.* 2004; Nguyen *et al.* 2007; Ball *et al.* 2010; Flechsig *et al.* 2010; Schütze *et al.* 2012a).

Secondly, fluid movements through porous media lead to the occurrence of electrokinetic effects. Naturally occurring electrical fields can be observed due to subsurface current sources induced by electrokinetic effects, electrochemical potential differences or thermoelectric coupling effects. This kind of effect is observable at e.g. hydrothermal systems and volcanoes (e.g., Lenat 2007; Lehto 2007; Revil *et al.* 2011) as well as by performing infiltration tests or subsurface flow in aquifers (e.g., Moore *et al.* 2005; Flechsig *et al.* 2008; Davis *et al.* 2010). In the latter case, the magnitude of streaming potential is generally low, being in the order of tens of millivolts (Bolève *et al.* 2009). The occurrence of concentration gradients caused by dissolution effects of volatile CO_2 in groundwater, as well as the movements of fluids through porous media driven by upward CO_2 migration, influence the measured potential differences. Obviously, it is very difficult to separate the various, simultaneous sources of SP signals in the measured data. However, SP maps can be used as an indicator of fluid flow processes in permeable geological structures and can also yield information on hydraulic properties. Byrdina *et al.* (2009) showed that measured SP and electrical resistivity tomography results are related to the permeable fracture zone which serves as a preferential pathway for soil gases and water.

An encouraging new approach for the comprehensive characterization of a gas-active fault is achieved by combining geophysical and soil-gas analysis methods (Schütze *et al.* 2012a). Such combinations have already been successfully used for the investigation of active volcanic or active hydrothermal regions (e.g., Revil *et al.* 2004, Finizola *et al.* 2009). Insights into structural and gas-dynamic features of a hydrothermally active fault were presented by Byrdina *et al.* (2009) using a combination of radon and CO_2 flux measurements at the surface with geoelectrical methods.

The application of the combined geophysical and soil-gas analysis methods for mesoscale monitoring of the shallow subsurface above geologic CO_2 storage sites can become a valuable tool for mapping and monitoring potential CO_2 spread in the subsurface. The combination of various kinds of geophysical information (such as resistivity, self-potential (SP) with surface-based measurements of CO_2 concentration and CO_2 flux) will help provide more reliable insights, in order to constrain the extent of potential leakages and to understand fluid flow patterns (Finizola *et al.* 2006; Schütze *et al.* 2012a).

Hence, the distribution of geophysical indicators in conjunction with observed characteristic CO_2 concentration patterns is considered useful for identifying particularly important locations where detailed investigations can be performed with the highest temporal and spatial resolution possible (as a subsequent level within the framework of a comprehensive monitoring concept).

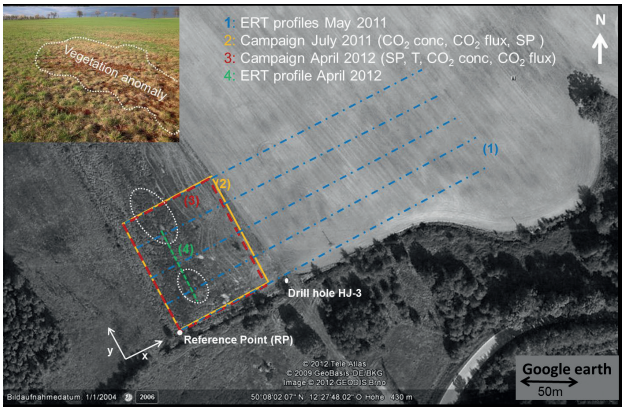

FIGURE 2

Measurement campaigns to characterize temporal and spatial variations of soil gas and to determine structural features carried out in May 2011, July 2011 and April 2012. The following data were measured: CO_2 concentration (mobile gas analyser ANSYCO GA94), CO_2 flux (Automated Soil CO_2 Flux System LI-8100A); DC (multi-electrode device RESECS) and self-potential (a pair of non-polarizable $Cu/CuSO_4$ electrodes and a high impedance voltmeter).

The measurements took place during three field campaigns to characterize temporal and spatial variations of soil gas and to determine structural features (Fig. 2).

Soil CO_2 concentration measurements

The soil-gas CO_2 concentration was measured in shallow soil horizons with typical sampling depths of 0.4 m (maximum) and with a sampling interval of 5 m. For this purpose, a mobile gas analyser ANSYCO GA94 was used to determine CO_2 and O_2 soil-gas concentrations. This device is able to detect these targets very quickly and reliably, with a maximum accuracy of 0.1%. This analysis is based on the infrared absorption behaviour of the soil-gas compounds. Typically, a single CO_2 concentration measurement takes only 30 seconds. All measured data showed distinct concentration patterns of increased CO_2 values coinciding with decreased O_2 concentrations. The data sets shown here were obtained during field campaigns in July 2011 and April 2012 (Fig. 2). Each data set consists of 200–250 concentration measurements.

Soil CO_2 flux measurement

CO_2 flux was measured using the accumulation chamber method with an Automated Soil CO_2 Flux System LI-8100A (LI-COR Biosciences). A small portion of air is circulated from a chamber into an infrared gas analyser (IRGA) and then sent back to the chamber with the aim of detecting CO_2 and H_2O concentrations. Carbon dioxide flux F_C is estimated using knowledge of the chamber volume, soil surface area, air temperature, atmospheric pressure, and the increasing CO_2 concentration C inside the chamber placed on to the soil surface for a short period of time t (dC/dt). At each sampling point all acquired concentration data $C(t)$ were used to fit the linear or exponential CO_2 flux rate functions with fitting quality parameter $\mathbf{R}^2 > 0.9$. The LI-COR 8100A allows a measurement range for CO_2 concentration of up to 20 000 ppm and H_2O concentrations of up to 60 ppt with a reading accuracy of 1.5%. The measurements were carried out using a survey chamber with a volume of 4843 cm^3 and a surface area of 317.8 cm^2. Additionally, the soil temperature was measured with a supplementary temperature sensor. Each sample measurement takes 5–10 minutes to perform, including the flushing procedure with ambient air. At sampling points with higher flux rates, the flushing period is adapted to avoid interaction with artefacts at subsequent sampling locations due to CO_2 residuals in the tubes.

The flux data were collected in two separate campaigns which took place in July 2011 and April 2012. These data sets include 72 and 65 samplings, respectively.

Self-Potential

Self-potential measurements were carried out with a pair of non-polarizable $Cu/CuSO_4$ electrodes. The offset error between the two electrodes was always less than 1 mV. This method measures the natural difference of electrical potential between two points directly at the ground surface. This potential difference is measured between the reference electrode ($x = 0$ m and $y = 0$ m) and a moving electrode with a high impedance voltmeter (resolution 0.1 mV, internal impedance 100 MOhm) and an isolated copper cable, 300-m long. At each station, an approximately 15-cm deep hole was dug to improve the electrical contact between the electrode and the ground ($R_c < 5$ kOhm). An additional reference dipole was installed to check potential daily variations and other influences on self-potential readings. Voltage variation rates at the reference dipole were very stable during one measurement campaign.

The spatial distribution of the naturally occurring potential difference pattern was observed in July 2011 and April 2012. The measurements were carried out simultaneously at the sampling locations where CO_2 concentration was measured. Subsequently, 200–250 self-potential readings were taken during each field campaign.

Geoelectrics

An ERT survey was carried out to provide a three-dimensional (3D) image of internal near surface structures. Data acquisition was performed on five 235-m parallel profiles with 5-m electrode spacing and 25-m line spacing, using the RESECS multi-electrode device (GeoServe, Germany). We applied Wenner-alpha, Wenner-beta, dipole-dipole and Schlumberger configurations along the profiles. These configurations are characterized by different signal-to-noise ratios and vertical resolutions. In particular, Wenner-alpha was used due to its advantageous signal-to-noise ratio, thereby allowing us to achieve measurements with larger offsets and to consider the requirement of higher sensitivity to vertical resistivity variations (Dahlin and Zhou 2004). Combinations with Wenner-beta and dipole-dipole configurations (both characterized by higher spatial resolu-

tions) utilize the higher sensitivity of this array to map 3D geological features in the subsurface.

Additionally, small-scale investigations with electrode spacing of 0.5 m were carried out along a 63.5-m profile with the aim of further investigating the shallow structures.

The measurements were carried out in May 2011 and April 2012. More than 10 300 data values were collected with a characteristic standard deviation error of 5%. After data pre-processing (including e.g. outlier filtering, injection current and voltage amplitude checks, filtering of measurements with erroneous electrodes), 80% of these values were used for the inversion process with BERT-code (boundless electrical resistivity tomography by Günther, Rücker and Spitzer 2006; Rücker, Günther and Spitzer 2006; www.resistivity.net/). The resistivity model was computed down to a maximum depth of 25 m, based on sensitivity analysis and depending upon the maximum length of the geoelectrical lines and the applied measurement configurations.

RESULTS AND INTERPRETATION

Soil CO_2 concentration measurements

Firstly, we consider the results of CO_2 concentration measurements carried out in July 2011 and April 2012 (Fig. 3). The distribution of CO_2 concentration shows variations spanning several orders of magnitude, from atmospheric values of 0.04–74%. Along the profiles, three types of zones can be distinguished according to CO_2 concentration ranges: (1) low CO_2 concentration (< 2% ± 0.5%), (2) medium concentration (3–10% ± 1%) and (3) high concentration peaks indicating focused CO_2 leakages (> 30% ± 3%). Comparison of measured data indicates that there are four key CO_2 leakage areas (x = 20 m y = 55 m, x = 20 m y = 65 m, x = 40 m y = 25 m, and x = 40 m y = 90 m) retrievable, while others seem to vary seasonally.

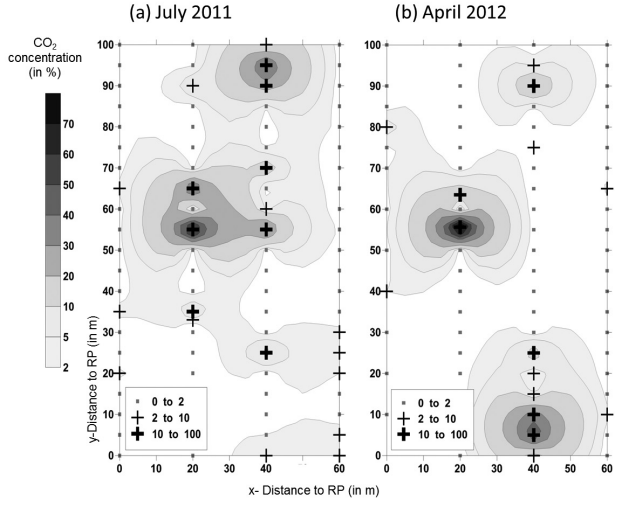

FIGURE 3

Results of the CO_2 concentration measurements with ASYNCO GA94 with a typical sampling depth of 0.4 m maximum: a) Logarithmic CO_2 concentration (in %) measured in July 2011; b) Logarithmic CO_2 concentration (in %) measured in April 2012.

The measurement results in Fig. 3 show distinct similarities but also significant differences. Several studies show that CO_2 in soils varies with time and depth and is influenced by factors such as soil water content, temperature, soil porosity, plant activity, soil organic carbon content, its degree of degradability and the availability of moisture and vegetation (Davidson and Trumbore 1995; Fang and Moncrieff 1999; Hamada and Tanaka 2001; Jassal *et al.* 2005; Flechard *et al*. 2007). Flechard *et al.* (2007) stated that soil moisture is a key controlling variable for soil CO_2 concentration. In addition, year-round monitoring is needed to distinguish CO_2 leakage from the highly variable natural biological CO_2 fluxes caused by microbial respiration and photosynthesis at the surface (Klusman 2003; Cortis, Oldenburg and Benson 2008). Furthermore, daily fluctuations and vertical distributions of CO_2 have been recorded for some mofettes and it should be noted that even degassing rates at natural analogues fluctuate and are not constant over time (van Gardingen *et al.* 1995; Vodnik *et al.* 2006).

The meteorological conditions during both measuring campaigns were quite similar. However, the soil degassing processes correlate with lower barometric pressure and impeding effects that occur due to higher soil moisture (Schütze *et al.* 2012b). Therefore, a single interpretation of CO_2 concentration measurements for indicating CO_2 leakages is difficult, since factors such as soil moisture, soil temperature and meteorological data (precipitation, temperature) greatly influence the degassing pattern.

Soil CO_2 flux measurement

In addition to CO_2 concentration, measurements of soil CO_2 fluxes are important, as CO_2 fluxes can act as a parameter of dynamic processes in the subsurface and can be used to describe the hazardous potential of degassing processes. The highest values of measured CO_2 flux rates exceeded 900 μmol m^{-2} s^{-1}, and the background value was determined from measured data and related references (Wagai *et al.* 1998; Chiodini *et al.* 2008) as being 6 μmol m^{-2} s^{-1}. The mean standard deviation for these flux measurements was estimated as being 20%. A correlation function determined for all obtained data is evident between flux rates and CO_2 concentration (Fig. 4). A significant positive correlation (R^2 = 0.93) between CO_2 concentration values greater than 3% (log CO_2 concentration > 0.5) and flux rates was determined. In contrast, concentration values below this threshold do not follow this relationship and are mainly influenced by biogenic soil processes. However, the magnitudes of the degassing anomalies vary strongly between the two measuring campaigns (Fig. 5).

The LI-COR 8100 accumulation chamber used allows further estimation of the mole fraction of water vapour in the considered gas volume and is used to indicate H_2O concentration. It can be used as an indicator of soil moisture at the sampling points. We normalized the measured values by the daily mean and show the

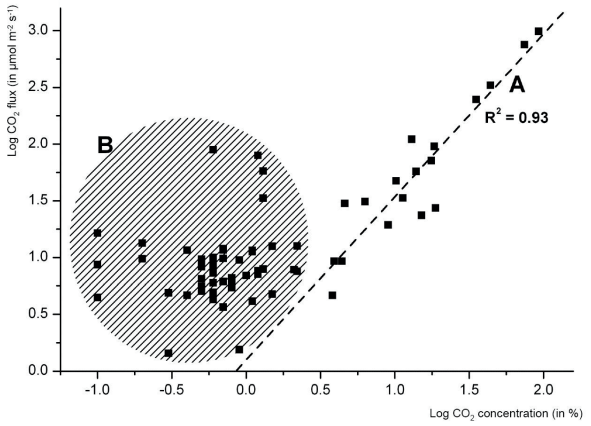

FIGURE 4

Correlation between logarithmic CO_2 concentration (in μmol **cm**$^{-2}$ **s**$^{-1}$) and logarithmic CO_2 fluxes (in %). A significant positive correlation (R^2 **= 0.93, A) between** CO_2 concentration values greater than 3% (log CO_2 concentration > 0.5) and increasing flux rates was determined. In contrast, concentration values below this threshold do not follow this relationship and are mainly influenced by biogenic soil processes (B).

correlation between H_2O and CO_2 flux for the measurements in July 2011 (Fig. 5a) and April 2012 (Fig. 5c). We observed quite different H_2O concentration effects in the accumulation chamber between these two measurements periods.

In July 2011, there were larger areas with increased H_2O concentration (in uppermost soil horizons) determined using the accumulation chamber method. We assume that high water content in the preferential soil-gas pathways generated a limited pore space for gas transport, which in turn led to increased gas pressure. This effect results in increased flux rates and an increased number of investigated degassing locations. Soil water is transported together with CO_2 gas. An increased H_2O concentration can be detected in the accumulation chamber. When 100% water saturation rates are achieved in the pores due to rainfall, a drop in flux rates is observable. The results of experiments carried out by Doff sotta *et al.* (2004) supports these findings, showing a 30% reduction in CO_2 flux rates and highlighting an increase in CO_2 concentrations immediately after a rainfall event. However, in April 2012, only one zone with increased H_2O concentration was observed between y = 15–35 m, where a distinct, positive SP anomaly was also measured. Figure 5 shows that there are generally lower flux rates compared to the flux rates in July 2011, with only a few prominent locations characterized by high degassing rates. The data measured in April 2012 indicated the occurrence of more diffuse degassing at the field site.

Some long-term soil-gas measurements that were recorded at an undisturbed location showed a strong correlation between soil-gas fluxes and soil moisture conditions as well as meteorological conditions.

Hashimoto and Komatsu (2006) pointed out that soil surface CO_2 flux rates responded to soil water content. Chiodini *et al.* (1998) recommend working in dry periods to avoid the influence

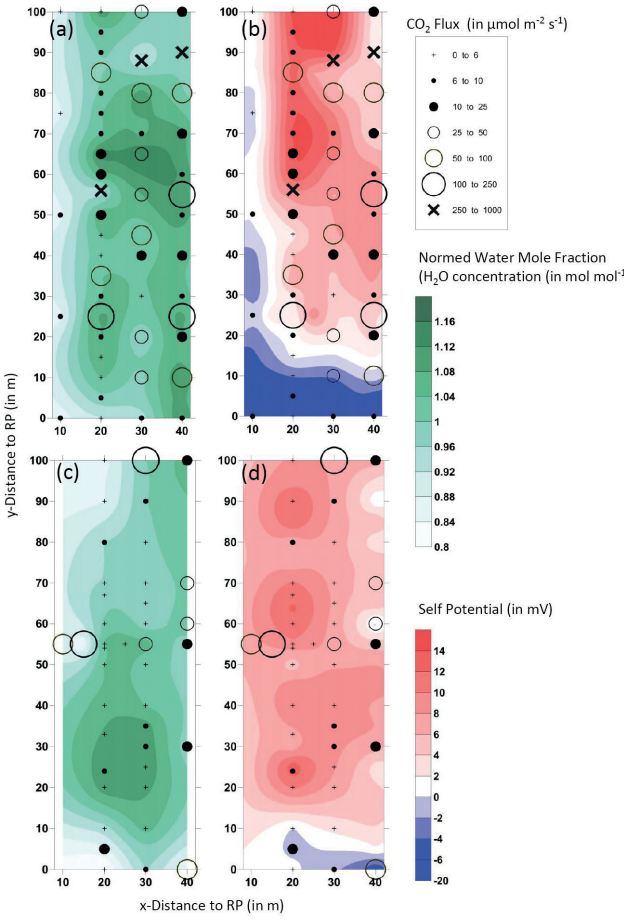

FIGURE 5

Comparison of normed water vapour mole fraction (H_2O concentration), CO_2 flux and self-potential measured in July 2011 and April 2012: a) Comparison of normed H_2O concentration (mol mol^{-1}) and CO_2 flux (μmol m^{-2} s^{-1}) measured in July 2011; b) Comparison of self-potential (mV) and CO_2 flux (μmol m^{-2} s^{-1}) measured in July 2011; c) Comparison of normed H_2O concentration (mol mol^{-1}) and CO_2 flux (μmol m^{-2} s^{-1}) measured in April 2012; d) Comparison of self-potential (mV) and CO_2 flux (μmol m^{-2} s^{-1}) measured in April 2012.

of rainfall and soil humidity. Unfortunately, this is not often possible in Central Europe.

Self-Potential

The measurements showed a typical SP range of between –20 mV to +14 mV with a standard deviation of 0.5 mV. In Fig. 5(b,d) the relationship between SP and CO_2 fluxes is analysed. A similarity in SP for both measuring campaigns was observed (Fig. 5b,d). The magnitudes of SP anomalies are in the same order. However, the pattern of these anomalies is slightly different. There are two distinct positive peaks x = 20 m y = 65 m and y = 95 m in Fig. 5(b), which can also attenuate in both campaigns. In contrast, an extension of the SP anomaly between x = 20–40 m y = 20–50 m (Fig. 5) was observed. In Fig. 5(b), the

area x = 0–40 m and y = 0–15 m is slightly influenced by groundwater discharge into the small drainage channel which is characterized by negative SP due to downward groundwater movement and is therefore difficult to interpret. The discharge effect in April 2012 (Fig. 5d) was considerably smaller than in July 2011 (Fig. 5b). Our measurements indicate no clear correlation between CO_2 fluxes and SP anomalies.

The measured SP pattern can be explained by a superposition of various effects: upward water flow driven by gas discharge and infiltration processes in unconsolidated sediments. Both positive and negative anomalies were found, thereby supporting the hypothesis that the water transport directions are different. Finizola *et al.* (2004) applied the SP method at active volcanoes and stated that along the structural features, short-wavelength SP minima can be interpreted in terms of water infiltration, and they coincide with CO_2 maxima interpreted in terms of preferential degassing paths along permeable faults. Resistivity, zeta potential and hydraulic parameters exert influence upon SP anomalies (Revil, Pezard and Glover 1999a; Revil *et al.* 1999b; Aizawa 2008). Hase *et al*. (2003) identified volcanic rocks that showed positive zeta potential in the Aso Caldera volcano, and suggested that a positive SP anomaly is explained not only by an upward flow but also by a combination of positive zeta potentials and downward flow. Revil *et al*. (1999b) identified positive zeta potentials for clay-rich materials. Byrdina *et al*. (2009) established a complex relationship between CO_2 flux and SP and described different SP types observed at zones with high CO_2 flux rates. Our results show that maximum CO_2 flux rates correlate with steps in SP data which are comparable to the results of the study carried out by Byrdina *et al*. (2009).

Generally, we assume a transport model where the upward migration of CO_2 is connected to additional transport of H_2O molecules in the same direction. This upward migration results in positive SP anomalies. At the points with highest flux rates (> 250 μmol m^{-2} s^{-1}) a drop in water content was observed compared to sampling points in the vicinity (Fig. 5a), which relates to disturbances in the positive SP pattern. Hence, we suppose that a joint transport of H_2O and CO_2 is responsible for positive SP anomalies. The observed SP pattern shows comparable characteristics to the results of the study carried out by Byrdina *et al.* (2009).

During performance of the measurements, we additionally discovered two typical processes with the accumulation chamber method (Fig. 7). The measurements in July 2011, characterized by higher flux rates, highlighted some locations (e.g., x = 30 m, y = 88 m) where CO_2 and water content actually increased during the determination of CO_2 fluxes in the chamber volume, resulting in high CO_2 fluxes (1000 μmol m^{-2} s^{-1}) and an increase in SP values. This water flux leads to decreased soil water content in the zones near to the degassing vents (as observed in our investigations). In contrast, in April 2012 there are certain locations (e.g., x = 40 m, y = 60 m) where decreasing water content and increasing CO_2 content is observed, resulting in moderate CO_2 fluxes (50 μmol m^{-2} s^{-1}) and decreased SP values. Considering the SP values, these typical effects confirm the assumptions made for aforementioned SP sources.

However, issues exist concerning the interpretation of the SP sources and the related processes and these need to be further investigated in laboratory experiments and with numerical simulations.

Geoelectrics

The variability of spatial resistivity within sedimentary layers is mostly related to changes in porosity, water saturation and/or the occurrence of clay minerals. Thus, an image of the resistivity distribution can be used to support the selection of interesting and significant sampling points for soil-gas analysis and for interpretation of the results obtained from these measurements. Furthermore, the analysis of resistivity anomalies is crucial when it comes to understanding the observed SP patterns.

Firstly, we applied a two-dimensional (2D) inversion on the five parallel profiles (including apparent resistivity data, which ranged from 5 to 650 Ω m). Then the results from all 2D inverted sections were combined to provide a quasi-3D resistivity image

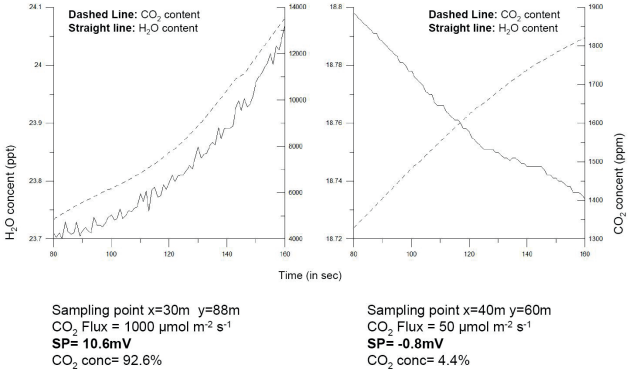

FIGURE 6

Results of geoelectrical measurements: a) 2D-inversion of the five parallel profiles including Wenner-alpha, Wenner-beta and Schlumberger data measured in May 2011 results in slices of subsurface resistivity distribution with significant structures; b) Lithostratigraphic layer description of borehole HJ-3. (Source: Czech Geological Survey, www.geofond.cz); c) Part of the 3D-inversion result of the Wenner-alpha data shows the model resistivity distribution at the surface in comparison to the determined soil degassing anomalies. A relationship between highly resistive structures and increased CO_2 concentration was not resolvable; d) Results of 2D-inversion of Wenner-alpha and dipole-dipole data obtained on a high-resolution ERT profile compared to mean CO_2 concentration (in %) measured along the profile at sampling depth of 40 cm and to the standard deviation derived from all measured soil-gas concentrations during the campaigns in 2011 and 2012. Structural features could be identified in the ERT section. CO_2 discharge into the atmosphere is mostly impeded by a thin conductive clay layer; significant variations in soil-gas accumulation could be explained by bulging and retention effects of the clayey surface layer due to the impact of meteoric water content.

of the subsurface (Fig. 6a). A slight topographic slope, which begins at a distance of x = 120 m, was incorporated into the inversion. The five resistivity model sections were calculated to a depth of 25 m below ground level. All sections were characterized by a heterogeneous resistivity distribution which depicts variations ranging from 25 to 1000 Ω m with a model misfit error of RMS = 20%. The inversion model presented a relatively high RMS error attributed to the contrast between maximum and minimum values of the input data justified by highly heterogeneous shallow structures. A thin top layer was widely evident and featured lower resistivities (with a mean value of 100 Ω m). Below this shallow conductive layer, characteristically resistive gully structures were observed with resistivity values greater than 600 Ω m. Distinct conductive structure anomalies with resistivities of less than 40 Ω m are apparent in depths of approx. 10 m below ground level. This specific resistivity distribution is traceable from the beginning of all profiles until inline coordinate x = 160 m. After this point, the layered structure is not present anymore, and a more or less homogeneous resistivity distribution of 60–120 Ω m in the subsurface is apparent.

The lithostratigraphic description of the 13.8-m deep HJ3 borehole (Czech Geological Survey, www.geofond.cz) supports ERT results. This borehole can be found at the edge of our investigation area (Fig. 6a,b). The ERT structures correspond to stratigraphic floodplain characteristics derived from the borehole. The upper soil horizon (to a depth of 1 m) is characterized by loamy and clayey mixed sediments, followed by an 8-m thick fluvial Quaternary sand and gravel layer with variable clay fractions. The Miocene Cypris clay bed is located 9 m below ground level. According to the stratigraphy results, the layered geoelectrical resistivity model reveals the presence of Quaternary and Miocene sediments. The soil water is highly mineralized and has a high HCO_3^- content (250 mg l^{-1}). The groundwater table was nearly stable at 2.50 m below surface level during all our measurements.

In Fig. 6(c) 3D inversion of the five parallel Wenner-alpha profiles is partially displayed. The inversion results show that 3D resistivity imaging is feasible and allows the carrying out of a spatial interpretation of ground conditions. The image shows a model of the resistivity distribution at surface level in the area where the detailed soil-gas and self-potential surveys took place. The area where degassing takes place can be characterized by a structured resistivity model (Fig. 6a,c). In particular, the intermediate highly resistant channels can be described as consisting of coarser sediments with lower clay content. This unconsolidated sediment layer seems to be defined by higher porosity levels and a greater number of interconnections; hence gas emissions may become more dispersed. The evidence of CO_2 concentration anomalies is often associated with regions of shallow zones of increased resistivities (Fig. 6c). However, a strong relation between CO_2 discharge locations and resistive areas could not be specified.

Additionally, a detailed representative ERT survey line with refined electrode spacing of 0.5 m was necessary to investigate near surface structures controlling CO_2 degassing behaviour. Figure 6(d) shows the joint inversion of the Wenner-alpha and dipole-dipole configurations down to a depth of 3 m compared with the CO_2 concentration distribution obtained along the profile from six measurements taken between 2011 and 2012. We

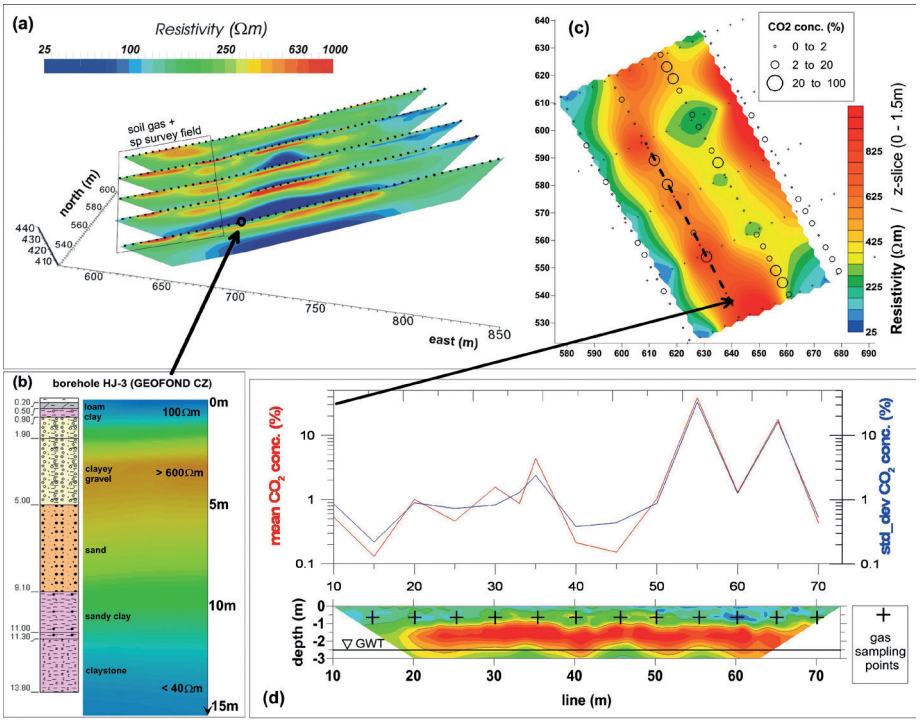

FIGURE 7
Temporal progress of CO_2 and H_2O content during a chamber measurement with the Automated Soil CO_2 Flux System LI-8100A (LI-COR Biosciences) at two sampling points with different flux behaviour.

observed strong deviations in the soil CO_2 concentration during all the measurements, which can be expressed in the standard deviation. We acquired highest CO_2 concentration values at locations x = 20 m and y = 55 and 65 m. However, these are also the locations with the strongest variations in measured soil-gas concentration values. To ascertain why this effect occurs, we considered the resistivity distribution beneath the profile. Structural features could be identified; a thin conductive top layer is covering a structure characterized by higher resistivities. In comparison to Fig. 6(b), these features are in accordance with the clayey, loamy sediments at the surface level followed by the gravel layer at a depth of 1 m. At a depth of 2.5 m, the resistivity values are slightly decreased due to the groundwater table.

The gas sampling locations were marked as (+) in Fig. 6(d) and measured at a depth of 40 cm. It is obvious that the sand and gravel layers are partly covered by a thin layer with lower gas permeability, due to higher clay content. CO_2 discharge into the atmosphere is mostly impeded by this thin clay layer. In the ERT result, a distinct zone is evident where the upper clay layer is only a few decimetres thin or nearly non-existent. Here, we can only observe moderate soil-gas concentrations, because a diffuse gas discharge into the atmosphere is possible in this zone. Higher CO_2 concentrations are determined in the sampling area between y = 50–70 m, where we observed conductive material at surface level and down to a depth of 1 m. The gas discharge into the atmosphere is impeded and we observed accumulation phenomena beneath this zone. Moreover, the gravel and sand layers act as reservoirs due to the gas-impermeable upper barrier. Significant variations in soil-gas accumulation could be explained by bulging and retention effects of the clayey surface layer due to the impact of meteoric water content in this layer. Further studies using small-scale geoelectrical monitoring at the discharge location are planned, with the objective of investigating the influence of the moist, uppermost clay horizon upon the degassing behaviour in more detail.

JOINT INTERPRETATION AND MODELLING

A relationship between geochemical and geophysical results at the analogue test site can be shown; however, interpretation of this information is quite complex. The results of the geoelectrical investigations give an insight into the structural features of the subsurface. CO_2 discharge into the atmosphere seems to be controlled by shallow thin clay-rich zones which were observed in the ERT results. However, structural features of the flow paths cannot be resolved with the recently presented measurements. With the help of SP measurement several transport processes can be identified. Results highlight the complex behaviour of temporal variations for these flow patterns. In particular, coupled migration of gas and water plays an important role.

Both the CO_2 concentration and CO_2 flux pattern can be described by distinct seasonal differences. In particular, the magnitude of the soil flux rates fluctuates by several orders. This can be explained by temporal changes in metrological and soil moisture conditions. Our measurements of CO_2 flux, CO_2 concentration and SP provide snapshots that highlight the prevalent conditions at a certain time. As previously described, soil moisture exerts great influence upon flux rates.

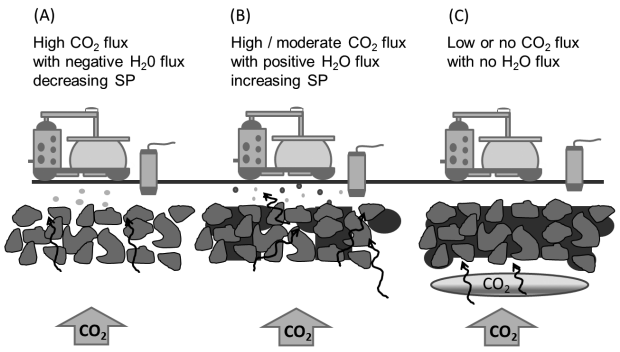

FIGURE 8
Three typical situations reflecting the varying measurement situations confronted with changing soil moisture conditions: (A) If pores are not filled with water the CO_2 can diffuse to the surface; measurement of high CO_2 fluxes and decreasing SP values; (B) Some pores 'dry up' and the soil is partly water saturated; measurement of moderate CO_2 fluxes and increasing SP values. The H_2O flux is an important influencing factor; (C) Pores get water saturated and act as a barrier for CO_2; CO_2 accumulation can occur beneath the water saturated zone and pore pressure can rise; measurement of low and no CO_2 fluxes, relation between flux and SP is not evident in our data.

We then must consider which kind of process is responsible for these observed effects. Using a general assumption that highly permeable sediments (sand and gravel) are found in the shallow subsurface, we can distinguish between three typical situations. (1) We assume that when preferential pathways are dry, CO_2 can diffuse through the pores and be transported directly to the surface and into the atmosphere. In this case, moderate to high CO_2 fluxes were measurable, and we could find the decreased SP signal (Case (A) in Fig. 8). (2) If the water evaporates due to meteorological conditions, some pores 'dry up' and the soil becomes partly saturated. H_2O is transported upward together with CO_2, and moderate to high CO_2 flux rates in combination with increased SP values were observable (Case (B) in Fig. 8). (3) Sometimes (e.g. after rain events or higher groundwater level) the pores become water saturated and act as a barrier for the CO_2. Therefore, the CO_2 cannot release and accumulates beneath this zone. With an increasing pressure of this accumulated CO_2 the possibility of the generation of small CO_2 migration paths rises and a sudden release can occur. However, this accumulation can take place at greater depths, not detectable with our measuring equipment for CO_2 concentration and CO_2 flux. Measurements by Rennert *et al.* (2011) at a natural analogue site showed at some locations increasing CO_2 concentration with greater depths (from 10 to 60 cm). These results correspond with our assumption (Case C). The data indicate low or no CO_2 fluxes and a relationship with SP anomalies is not evident.

Doff sotta *et al.* (2004) reported that measured CO_2 concentration gradient in the soil profile shows an accumulation of concentration for CO_2 after a rainfall event on the top soil. This higher CO_2 concentration developed shortly after rainfall when the soil pores in the upper layers were filled with water, which created a barrier for gas exchange between the soil and the atmosphere. Hence, gas concentration mapping in greater depths using direct-push methods is considered to be essential, allowing the analysis of fault systems, as well as inward migration of gases into the sediments (Schütze *et al.* 2012a). The degassing behaviour of clay-rich sediment layers with lower permeability at the surface can be described in a comparable manner. A higher clay fraction in the sediments decreases the permeability and impedes gas migration, just as H_2O does. However, temporal variations can be neglected. A correlation between the thickness of the upper clay layer and CO_2 flux rates is discussed by Schütze *et al.* (2012b).

We propose a conceptual model (illustrated in Fig. 9) derived from shallow ERT results shown in Fig. 6(d) and soil-gas measurements. With this model, the influence of different permeability structures at the near surface on degassing processes is studied to find a first explanation for the observed CO_2 concentration pattern.

The model (Fig. 9) has a thin inhomogeneous zone, which is in a 15-m upper sandy layer located above a clay layer penetrated by a vertical fault. The inhomogeneity is conceptually represented by a zone situated horizontally in the centre of the sandy layer. This zone is 2-m long and consists of a spatially isolated area of lower permeability (e.g. by higher clay or water content). CO_2 rich gas (99%) is continuously supplied into the sandy zone through the fault with an inflow rate 1×10^{-3} m s^{-1}. This first model is assumed to be situated in the vadose zone and only CO_2 transportation is present in the gaseous phase. These boundary conditions focus on the impacts of inhomogeneous permeability zones on CO_2 gas flow. Various permeability contrasts were implemented in the inhomogeneous zone in order to study their influence upon CO_2 concentrations near the ground surface, and to simulate different permeability conditions. Steady-state transport processes of a gas mixture (air and CO_2) under isothermal conditions (15°C) are modelled assuming a half space of the symmetric domain using the finite element code OpenGeoSys (Singh, Görke and Kolditz 2011; Singh *et al.* 2012). Effective porosity is set at 0.2 in all zones and the CO_2 molecular diffusion coefficient in air is set to 1.39×10^{-5} m^2 s^{-1} (Pritchard and Currie 1982). CO_2 concentration at the ground surface is fixed to the ambient atmospheric concentration value.

This conceptual model can be used to consider two scenarios: firstly, variable zone extension with fixed permeability ($1.0 \times 10e^{-12}$) and secondly, variable permeability ($1.0 \times 10e^{-12} - 1.0 \times 10e^{-15}$ m^2) with fixed zone extension (2 m). However, the permeability of the preferential path has a larger impact on measured CO_2 gas concentrations than the zone extension has. Therefore, we focused on the influence of the low permeability zone on the results of the conceptual model.

Figure 9 shows CO_2 concentrations along profiles determined at a depth of 0.5 m below the ground surface. These concentration profiles are calculated for various ratios of inhomogeneous zone permeability (k) to the sand permeability ($k_{sand} = 10^{-12}$ m^2). A typical profile for a homogeneous case is presented in Fig. 9 where $k/k_{sand} = 1$ (see curve A). In the homogeneous case for $k/k_{sand} = 1$ (case A) maximum concentration of CO_2 is observed

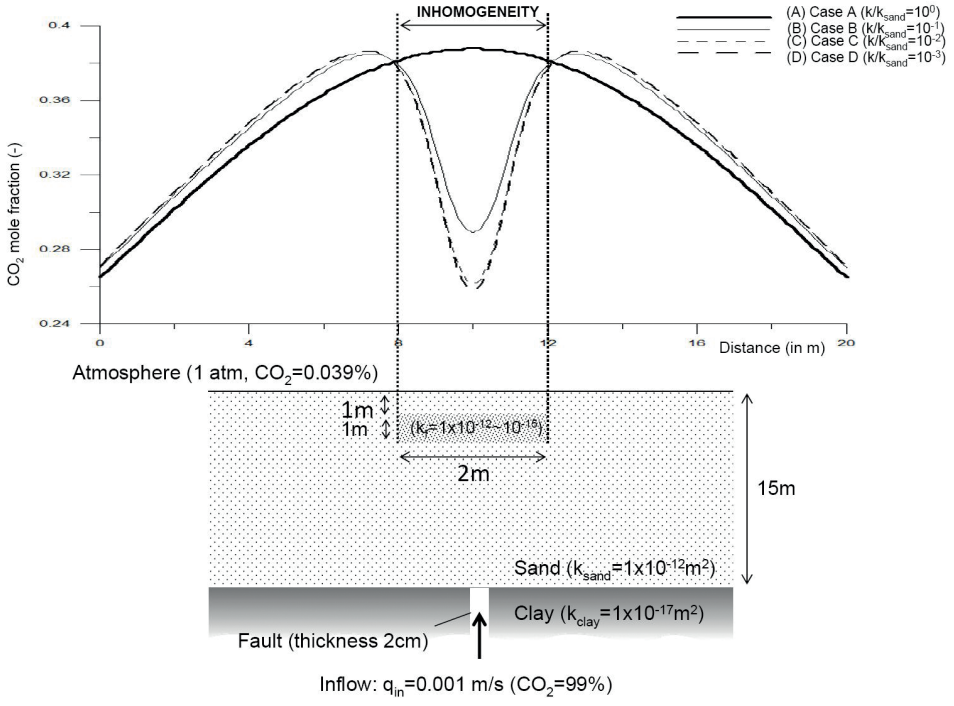

FIGURE 9
Conceptual model with an inhomogeneous zone of 2 m and simulated results showing horizontal profile of CO_2 mole fraction at depth 0.5 m.

above the fault (x = 0 m) and decreases with increased fault distance. In comparison, the peak location and its concentration maximum change when an inhomogeneous zone is introduced in the model (curve B-D). In this case, the concentration above the fault converges to a value forming a local minimum (curve B-D) and the CO_2 concentration maximum is located at the outer edges of the inhomogeneous zone. For our assumed model the concentration maximum is shifted approximately 2 m from the border of the inhomogeneous zone. The observed maximum above the CO_2 fault falls from 39% (Case A) to 29% (Case B) and 26% (Case C and D). Kolditz *et al.* (2012) applied a similar model with a 10-m zone extension in a greater depth and results show almost the same curve progression as the previously described model. If the assumed inhomogeneous zone is located deeper, then results show greater horizontal extent in the observed induced concentrations near the ground surface.

The modelling results imply that having precise knowledge of permeability distributions in the sand layer is important when it comes to interpreting measured soil CO_2 gas concentrations. The presence of low permeability zones (e.g., clay rich or water saturated) has a great effect upon the location of the highest CO_2 concentrations. Furthermore, this first conceptual model shows that a diffuse degassing behaviour is strongly correlated with the permeability contrasts in the near surface structures. This can be influenced e.g. by temporary changes in soil moisture content, thereby confirming our observed results. The obtained measured and modelled results suggest that gas uprising is much localized around restricted areas, often controlled by local permeability contrasts. Thus, different geophysical methods as well as soil-gas measurements can provide important information about degassing characteristics.

CONCLUDING REMARKS

Naturally occurring CO_2 deposits provide unique natural analogues which can be used to evaluate the long-term safety and efficacy of storing anthropogenic CO_2 in geologic formations. The investigation of natural CO_2 release sites can facilitate the attainment of valuable information that can help us better understand the chemical and physical processes taking place and thus provide useful information for the development of new monitoring and assessment tools. Furthermore, natural analogues help provide reliable insights into processes related to CO_2 migration, trapping and leakage. The Cheb Basin is a convenient natural analogue site for comprehensive study of upward CO_2 migration and surface leakages because various forms of CO_2 degassing processes occur at this site. It offers the possibility of verifying appropriate monitoring tools used for the direct investigation of processes along preferential migration paths. The CO_2-rich mineral springs and mofettes along the major faults are an indication of preferential CO_2 migration pathways. They are supplied by fluids from a deep magmatic reservoir in the lithospheric mantle. A joint application of geophysical information such as resistivity, self-potential with surface-based measurements of CO_2 concentration and CO_2 flux can provide more reliable insights which help constrain the extent of potential leakage systems and helps us to understand the fluid flow pattern with strong dependency on soil conditions. Apart from soil conditions, the thickness and permeability of site-specific near surface sedimentary deposits have a great influence upon the spatial distribution of CO_2 degassing patterns at surface level. Soil-gas surveys in combination with geophysical investigations have been proven to be a valuable tool for the characterization of near surface structural features controlling the degassing process. Depending on the required spatial and temporal resolution, method combination is recommended for the characterization and observation of medium to small-scale areas (not larger than 500 m × 500 m).

A large-scale ERT survey is necessary to gain overall information about subsurface structures. As such, we recommend that small-scale time-lapse monitoring with a dense electrode grid is used to investigate near surface structures controlling CO_2 degassing behaviour. Our results show that near surface structures and the interactions between sediment, gas and water in the vadose zone greatly influence degassing processes. These processes may reveal resistivity distribution variations which are observable with ERT monitoring. Time-lapse ERT results can provide the information required for interpretation of SP, CO_2 flux and soil-gas concentration data. For further monitoring, a comprehensive observation set-up should be established that includes SP, time-lapse ERT, meteorological parameters and soil-gas measurements.

Site-specific near surface geological features and meteorological conditions seem to exert great influence upon degassing patterns. In this current study, the distribution and thickness of low permeability sediments at surface level and soil moisture conditions have been shown to impede CO_2 discharge into the atmosphere. Moreover, this layer is also responsible for CO_2 accumulation in the porous sediment layer underneath. Hence, the measured CO_2 soil-gas concentrations and fluxes relate to the environmental conditions at the time of measurement. Therefore, they represent a snapshot with both a distinct typical pattern and certain differences caused by soil and meteorological conditions. Permanent monitoring of CO_2 is a prerequisite to developing effective monitoring concepts for CO_2 leakages.

Great effort is required for monitoring CO_2 fluxes at larger scales with the devices available now. Hence, finding proxies for permanent monitoring is a prerequisite to developing effective monitoring concepts for CO_2 leakages. SP measurements are able to reflect the dynamic processes; however, the presented results show clearly that further research is essential.

ACKNOWLEDGEMENTS

The presented work has been funded by the German Federal Ministry of Education and Research (BMBF) in the frame of the GEOTECHNOLOGIEN Program, and the financial support for the projects MONACO (grant ID: 03G0785A) and CO2BENCH (grant ID: 03G0797D) is gratefully acknowledged. Finally, we cordially thank our native speaker Christopher Higgins for proofreading the manuscript.

REFERENCES

Aizawa K. 2008. Classification of self-potential anomalies on volcanoes and possible interpretations for their subsurface structure. *Journal of Volcanology and Geothermal Research* **175**, 253–268. doi:10.1016/j.jvolgeores.2008.03.011

Annunziatellis A., Beaubien S.E., Bigi S., Ciotoli G., Coltella M. and Lombardi S. 2008. Gas migration along fault systems and through the vadose zone in the Latera caldera (central Italy): implications for CO_2 geological storage. *International Journal of Greenhouse Gas Control* **2**, 353–372. doi: 10.1016/j.ijggc.2008.02.003

Ball L., Ge S., Caine J., Revil A. and Jardani A. 2010. Constraining faultzone hydrogeology through integrated hydrological and geoelectrical analysis. *Hydrogeology Journal* **18**, 1057–1067. doi: 10.1007/s10040-010-0587-z

Bankwitz P., Schneider G., Kämpf H. and Bankwitz E. 2003. Structural characteristics of epicentral areas in Central Europe: study case Cheb Basin (Czech Republic). *Journal of Geodynamics* **35**, 5–32. doi: 1016/S0264-3707(02)00051-0

Battani A., Deville E., Faure J.L., Jeandel E., Noirez S., Tocqué E. *et al*. 2010. Geochemical study of natural CO_2 emissions in the French Massif Central: how to predict origin, processes and evolution of CO_2 leakage. *Oil & Gas Science and Technology – Revue d'IFP Energies nouvelles* **65**, 615–633. doi: 10.2516/ogst/2009052

Bennati L., Finizola A., Walker J.A., Lopez D.L., Higuera-Diaz I.C., Schütze C. *et al*. 2011. Fluid circulation in a complex volcano-tectonic setting, inferred from self-potential and soil CO_2 flux surveys: The Santa María-Cerro Quemado-Zunil volcanoes and Xela caldera (Northwestern Guatemala). *Journal of Volcanology and Geothermal Research* **199**(3–4), 216–229. doi: 10.1016/j.jvolgeores.2010.11.008

Bolève A., Revil A., Janod F., Mattiuzzo J.L. and Fry J.-J. 2009. Preferential fluid flow pathways in embankment dams imaged by self-potential tomography. *Near Surface Geophysics* **7**(5), 447–462. doi: 10.3997/1873-0604.2009012

Börner J.H., Herdegen V., Repke J.-U. and Spitzer K. 2012. The impact of CO_2 on the electrical properties of water bearing porous media – laboratory experiments with respect to carbon capture and storage. *Geophysical Prospecting* **61**. doi: 10.1111/j.1365-2478.2012.01129.x

Bräuer K., Kämpf H., Niedermann S., Strauch G. and Tesar J. 2008. Natural laboratory NW Bohemia: Comprehensive fluid studies between 1992 and 2005 used to trace geodynamic processes. *Geochemistry Geophysics Geosystems* **9**, Q04018. doi:10.1029/2007GC001921

Bräuer K., Kämpf H., Koch U. and Strauch G. 2011. Monthly monitoring of gas and isotope compositions in the free gas phase at degassing locations close to the Nový Kostel focal zone in the western Eger Rift, Czech Republic. *Chemical Geology* **290**, 163–176. doi: 10.1016/j.chemgeo.2011.09.012

Byrdina S., Revil A., Pant S.R., Koirala B.P., Shrestha P.L., Tiwari D.R. *et al*. 2009. Dipolar self-potential anomaly associated with carbon dioxide and radon flux at Syabru-Bensi hot springs in central Nepal. *Journal of Geophysical Research: Solid Earth* **114**, B10101. doi: 10.1029/2008JB006154

Carapezza M.L., Ricci T., Ranaldi M. and Tarchini L. 2009. Active degassing structures of Stromboli and variations in diffuse CO_2 output related to the volcanic activity. *Journal of Volcanology and Geothermal Research* **182**, 231–245. doi: 10.1016/j.jvolgeores.2008.08.006

Chiodini G., Cioni R., Guidi M., Marini L. and Raco B. 1998. Soil CO_2 flux measurements in volcanic and geothermal areas. *Applied Geochemistry* **13**, 543–552. doi: 10.1016/S0883-2927(97)00076-0

Chiodini G., Caliro S., Cardellini C., Avino R., Granieri D. and Schmidt A. 2008. Carbon isotopic composition of soil CO_2 efflux, a powerful method to discriminate different sources feeding soil CO_2 degassing in volcanic-hydrothermal area. *Earth and Planetary Science Letters* **274**, 372–379.

Ciotoli G., Etiope G., Guerra M. and Lombardi S. 1999. The detection of concealed faults in the Ofanto Basin using the correlation between soil-gas fracture surveys. *Tectonophysics* **301**, 321–332. doi: 10.1016/S0040-1951(98)00220-0

Cortis A., Oldenburg C.M. and Benson S.M. 2008. The role of optimality in characterizing CO_2 seepage from geologic carbon sequestration sites. *International Journal of Greenhouse Gas Control* **2**, 640–652. http://escholarship.org/uc/item/4bx404p5

Dahlin T. and Zhou B. 2004. A numerical comparison of 2D resistivity imaging with 10 electrode arrays. *Geophysical Prospecting* **52**, 379–398.

Davidson E.A. and Trumbore S.E. 1995. Gas diffusivity and production of CO_2 in deep soils of the eastern Amazon. *Tellus* **47B**, 550–565.

Davis C.A., Slater L.D., Kulessa B., Ferguson A., Atekwana E.A., Doherty R. and Kalin R. 2010. Self-potential signatures associated with an injection experiment at an in-situ biological permeable reactive barrier. *Near Surface Geophysics* **8**, 541–551. doi: 10.3997/1873-0604.2010034

Doff Sotta E., Meir P., Malhi Y., Donato Nobre A., Hodnett M. and Grace J. 2004. Soil CO_2 efflux in a tropical forest in the central Amazon. *Global Change Biology* **10**, 601–617. doi:10.1111/j.1529-8817.2003.00761.x

Etiope G. and Lombardi S. 1995. Evidence for radon transport by carrier gas through faulted clays in Italy. *Journal of Radioanalytical and Nuclear Chemistry* **193**, 291–300. doi: 10.1007/BF02039886.

Etiope G., Guerra M. and Raschi A. 2005. Carbon dioxide and radon geohazards over a gas-bearing fault in the Siena Graben (Central Italy). *Terrestrial Atmospheric and Oceanic Sciences* **16**, 885–896.

European Parliament and the Council. 2009. DIRECTIVE 2009/31/EC OF THE EUROPEAN PARLIAMENT AND OF THE COUNCIL of 23 April 2009 on the geological storage of carbon dioxide and amending Council Directive 85/337/EEC, European Parliament and Council Directives 2000/60/EC, 2001/80/EC, 2004/35/EC, 2006/12/EC, 2008/1/EC and Regulation (EC) No 1013/2006.

Fang C. and Moncrieff J.B. 1999. A model for soil CO_2 production and transport 1: Model development. *Agricultural and Forest Meteorology* **95**, 225–236. doi: 10.1016/S0168-1923(99)00036-2

Finizola A., Lenat J.-F., Macedo O., Ramos D., Thouret J.-C. and Sortino F. 2004. Fluid circulation and structural discontinuities inside Misti volcano (Peru) inferred from self-potential measurements. *Journal of Volcanology and Geothermal Research* **135**, 343–360. doi: 10.1016/j.jvolgeores.2004.03.009

Finizola A., Revil A., Rizzo E., Piscitelli S., Ricci T., Morin J. *et al*. 2006. Hydrogeological insights at Stromboli volcano (Italy) from geoelectrical, temperature, and CO_2 soil degassing investigations. *Geophysical Research Letters* **33**, L17304. doi: 10.1029/2006GL026842

Finizola A., Aubert M., Revil A., Schütze C. and Sortino F. 2009. Importance of structural history in the summit area of Stromboli during the 2002–2003 eruptive crisis inferred from temperature, soil CO_2, self-potential, and electrical resistivity tomography. *Journal of Volcanology and Geothermal Research* **183**, 213–227. doi:10.1016/j.jvolgeores.2009.04.002

Flechard C.R., Neftel A., Jocher M., Ammann C., Leifeld J. and Fuhrer J. 2007. Temporal changes in soil pore space CO_2 concentration and storage under permanent grassland *Agricultural and Forest Meteorology* **142**, 66–84. doi: 10.1016/j.agrformet.2006.11.006.

Flechsig Ch., Bussert R., Rechner J., Schütze C. and Kämpf H. 2008. The Hartousov mofette field in the Cheb Basin, Western Eger Rift (Czech Republic): a comparative geoelectric, sedimentologic and soil gas study of a magmatic diffuse CO_2-degassing structure. *Zeitschrift für Geologische Wissenschaften* **36**, 177–193.

Flechsig Ch., Fabig T., Rücker C. and Schütze C. 2010. Geoelectrical investigations in the Cheb Basin/W-Bohemia: An approach to evaluate the near-surface conductivity structure. *Studia Geophysica et Geodaetica* **54**, 443–463.

Gal F., Michel B., Gilles B., Frédéric J. and Karine M. 2011. CO_2 escapes in the Laacher See region, East Eifel, Germany: Application of natural analogue onshore and offshore geochemical monitoring. *International Journal of Greenhouse Gas Control* **5**(4), 1099–1118. doi:10.1016/j.ijggc.2011.04.004

Günther T., Rücker C. and Spitzer K. 2006. Three-dimensional modelling and inversion of dc resistivity data incorporating topography – II. Inversion. *Geophysical Journal International* **166**, 506–517. doi: 10.1111/j.1365-246X.2006.03011.x

Hamada Y. and Tanaka T. 2001. Dynamics of carbon dioxide in soil profiles based on long-term field observation. *Hydrological Processes* **15**, 1829–1845. doi:10.1002/hyp.242

Hase H., Ishido T., Takakura S., Hashimoto T., Sato K. and Tanaka Y. 2003. ζ-potential measurement of volcanic rocks from Aso caldera. *Geophysical Research Letters* **30**(23), 2210. doi:10.1029/2003GL018694

Hashimoto S. and Komatsu H. 2006. Relationships between soil CO_2 concentration and CO_2 production, temperature, water content, and gas diffusivity: implications for field studies through sensitivity analyses. *Journal of Forest Research* **11**(1), 41–50. doi: 10.1007/s10310-005-0185-4

Hoffmann R. and Dietrich P. 2004. An approach to determine equivalent solutions to the geoelectrical 2D inversion problem. *Journal of Applied Geophysics* **56**, 79–91.

Holloway S., Pearce J.M., Hards V.L., Ohsumi T. and Gale J. 2007. Natural emissions of CO_2 from the geosphere and their bearing on the geological storage of carbon dioxide. *Energy* **32**, 1194–1201. doi: 10.1016/j.energy.2006.09.001

Itaoka K., Saito A. and Akai M. 2004. Public Acceptance of CO_2 Capture and Storage Technology: A Survey of Public Opinion to Explore Influential Factors. In: *Proceedings of 7th International Conference on Greenhouse Gas Control Technologies. IEA Greenhouse Gas Programme*, v. 1, (eds E.S. Rubin, D.W. Keith and C.F. Gilboy). Peer-Reviewed Papers and Overviews, Elsevier, Oxford.

Jarvis A., Reuter H.I., Nelson A. and Guevara E. 2008. Hole-filled SRTM for the globe Version 4, available from the CGIAR-CSI SRTM 90m Database (http://srtm.csi.cgiar.org).

Jassal R., Black A., Novak M., Morgenstern K., Nesic Z. and Gaumont-Guay D. 2005. Relationship between soil CO_2 concentrations and forest-floor CO_2 effluxes. *Agricultural and Forest Meteorology* **130**, 176–192. doi: 10.1016/j.agrformet.2005.03.005

Johansson S., Rosqvist H., Svensson M., Dahlin T. and Leroux V. 2011. An alternative methodology for the analysis of electrical resistivity data from a soil gas study. *Geophysical Journal International* **186**, 632–640. doi: 10.1111/j.1365-246X.2011.05080.x

Kämpf H., Bräuer K., Schumann J., Hahne K. and Strauch G. 2012. CO_2 discharge in an active, non-volcanic continental rift area (Czech Republic): Characterisation (δ13C, 3He/4He) and quantification of diffuse and vent CO_2 emissions. *Chemical Geology* **339**, 71–83. doi: 10.1016/j.chemgeo.2012.08.005

Kharaka Y.K., Thordsen J.J., Kakouros E., Ambats G., Herkelrath W.N., Birkholzer J.T., Apps J.A. *et al*. 2010. Changes in the Chemistry of Shallow Groundwater Related to the 2008 Injection of CO_2 at the ZERT Field Site, Bozeman, Montana. *Environmental Earth Sciences* **60**(2), 273-284. doi: 10.1007/s12665-009-0401-1

Klusman RW. 2003. Rate measurements and detection of gas microseepage to the atmosphere from an enhanced oil recovery/sequestration project, Rangely, Colorado, USA. *Applied Geochemistry* **18**, 1825–1838. doi: 10.1016/S0883-2927(03)00108-2

Kolditz O., Bauer S., Beyer C., Böttcher N., Dietrich P., Görke U.-J. *et al*. 2012. A systematic benchmarking approach for geologic CO_2 injection and storage. *Environmental Earth Sciences* **67**(2), 613–632. doi:10.1007/s12665-012-1656-5

Lamert H., Geistlinger H., Werban U., Schütze C., Peter A., Hornbruch G. *et al*. 2012. Feasibility of geoelectrical monitoring and multiphase modeling for process understanding of gaseous CO_2 injection into a shallow aquifer. *Environmental Earth Sciences* **67**(2). doi: 10.1007/s12665-012-1669-0

Lehto H.L. 2007. *Self-Potential Anomalies and CO_2 Flux on Active Volcanoes: Insights from Time and Spatial Series at Masaya, Telica, and Cerro Negro.* Nicaragua Thesis of Master of Science, Department of Geology, College of Arts and Sciences University of South Florida. URL: http://digital.lib.usf.edu:8080/fedora/get/usfldc:E14-SFE0002108/DOCUMENT

Lenat J.-F. 2007. Retrieving self-potential anomalies in a complex volcanic environment: an SP/elevation gradient approach. *Near Surface Geophysics* **5**(3), 161–170. doi: 10.3997/1873-0604.2006028

Lewicki J.L., Connor C., St-Amand K., Stix J. and Spinner W. 2003. Self-potential, soil CO_2 flux, and temperature on masaya volcano, nicaragua. Lawrence Berkeley National Laboratory: Lawrence Berkeley National Laboratory. URL: http://escholarship.org/uc/item/1m89q9hr

Lewicki J.L., Oldenburg C.M., Dobeck L. and Spangler L. 2007. Surface CO_2 leakage during two shallow subsurface CO_2 releases. *Geophysical Research Letters* **34**, L24402. doi: 101029/2007GL032047.

McCoy S.T and Rubin E.S. 2005. Models of CO_2 Transport and Storage Costs and Their Importance in CCS Cost Estimates. In: *Proceedings of the 4th Annual Conference on Carbon Capture and Sequestration*, Alexandria, VA, 2005.

Moore J., Adams M., Allis R., Lutz S. and Rauzi S. 2005. Mineralogical and geochemical consequences of the long-term presence of CO_2 in natural reservoirs: an example from the Springerville-St. Johns Field, Arizona, and New Mexico, USA. *Chemical Geology* **217**, 365–385. doi: 10.1016/j.chemgeo.2004.12.019

Nguyen F., Garambois S., Chardon D., Hermitte D., Bellier O. and Jongmans O. 2007. Subsurface electrical imaging of anisotropic formations affected by a slow active reverse fault, Provence, France. *Journal of Applied Geophysics* **62**, 338–355. doi: 10.1016/j.jappgeo.2007.03.003.

Norden B. 2011. Modelling of the near-surface groundwater flow system at the CO2SINK site Ketzin, Germany, Zeitschrift der Deutschen Gesellschaft für Geowissenschaften (ZDGG) Band 162 Heft 1, 63–77. doi: 10.1127/1860-1804/2011/0162-0063

Pettinelli E., Beaubien S.E., Zaja A., Menghini A., Praticelli N., Mattei E. *et al*. 2010. Characterization of a CO_2 gas vent using various geophysical and geochemical methods. *Geophysics* **75**, B137–B146. doi: 10.1190/1.3420735.

Pritchard D.T. and Currie J.A. 1982. Diffusion of coefficients of carbon dioxide, nitrous oxide, ethylene and ethane in air and their measurement. *Journal of Soil Science* **33**, 175–184. doi: 10.1111/j.1365-2389.1982.tb01757.x

Rein A., Hoffmann R. and Dietrich P. 2004. Influence of natural timedependent variations of electrical conductivity on DC resistivity measurements. *Journal of Hydrology* **285**(1–4), 215–232. doi:10.1016/j.jhydrol.2003.08.015

Rennert T., Eusterhues K., Pfanz H. and Totsche K.U. 2011. Influence of geogenic CO_2 on mineral and organic soil constituents on a mofette site in the NW Czech Republic. *European Journal of Soil Science* **62**, 572–580. doi: 10.1111/j.1365-2389.2011.01355.x

Revil A., Pezard P.A. and Glover P.W.J. 1999a. Streaming potential in porous media. 1. Theory of the zeta-potential. *Journal of Geophysical Research* **104**(B9), 20,021–20,031. doi: 10.1029/1999JB900089.

Revil A., Schwaeger H., Cathles L.M. and Manhardt P. 1999b. Streaming potential in porous media. 2. Theory and application to geothermal systems. *Journal of Geophysical Research* **104**(B9), 20,033–20,048. doi: 10.1029/1999JB900090

Revil A., Finizola A., Sortino F. and Ripepe M. 2004. Geophysical investigations at Stromboli volcano, Italy. Implications for ground water flow. *Geophysical Journal International* **157**, 426–440. doi: 10.1111/ j.1365-246X.2004.02181.x

Revil A., Finizola A., Ricci T., Delcher E., Peltier A., Barde-Cabusson S. *et al*. 2011. Hydrogeology of Stromboli volcano, Aeolian Islands (Italy) from the interpretation of resistivity tomograms, self-potential, soil temperature and soil CO_2 concentration measurements. *Geophysical Journal International* **186**, 1078–1094. doi: 10.1111/ j.1365-246X.2011.05112.x

Rücker C., Günther Th. and Spitzer K. 2006. Three-dimensional modelling and inversion of dc resistivity data incorporating topography-I. Modelling. *Geophysical Journal International* **166**, 495–505. doi:10.1111/j.1365-246X.2006.03010.x

Sauer U., Schütze C., Leven C., Schlömer S. and Dietrich P. 2013. An integrative hierarchical monitoring approach applied at a natural analogue site to monitor CO_2 degassing areas. *Acta Geotechnica*, 1–7. doi:10.1007/s11440-013-0224-9

Schütze C., Vienken T., Werban U., Dietrich P., Finizola A. and Leven C. 2012a. Joint application of geophysical methods and Direct Push-soil gas surveys for the improved delineation of buried fault zones. *Journal of Applied Geophysics* **82**, 129–136. doi: 10.1016/j.jappgeo.2012.03.002

Schütze C., Sauer U., Beyer K., Lamert H., Bräuer K., Strauch G. *et al*. 2012b. Natural analogues – a potential approach for developing reliable monitoring methods to understand subsurface CO_2 migration processes. *Environmental Earth Sciences* **67**. doi: 10.1007/s12665-012-1701-4

Singh A.K., Görke U.J. and Kolditz O. 2011. Numerical simulation of non-isothermal compositional gas flow: Application to carbon dioxide injection into gas reservoirs. *Energy* **36**, 3446–3458. doi: 10.1016/j.energy.2011.03.049

Singh A.K., Baumann G., Henninges J., Görke U.J. and Kolditz O. 2012. Numerical analysis of thermal effects during carbon dioxide injection with enhanced gas recovery: a theoretical case study for the Altmark gas field. *Environmental Earth Sciences* **67**. doi: 10.1007/s12665-012-1689-9

van Gardingen P.R., Grace J., Harkness D.D., Miglietta F. and Raschi A. 1995. Carbon dioxide emissions at an Italian mineral spring: measurements of average CO_2 concentration and air temperature. *Agricultural and Forest Meteorology* **73**, 17–27. doi: 10.1016/0168-1923(94)02176-K

Vodnik D., Kastelec D., Pfanz H., Maček I. and Turk B. 2006. Small-scale spatial variation in soil CO_2 concentration in a natural carbon dioxide spring and some related plant responses. *Geoderma* **133**(3–4), 309–319. doi:10.1016/j.geoderma.2005.07.016

Voltattorni N., Sciarra A., Caramanna G., Cinti D., Pizzino L. and Quattrocchi F. 2009. Gas geochemistry of natural analogues for the studies of geological CO_2 sequestration. *Applied Geochemistry* **24**, 1339–1346. doi:10.1016/j.apgeochem.2009.04.026

Wagai R., Brye K.R., Gower S.T., Norman J.M. and Bundy L.G. 1998. Land use and environmental factors influencing soil surface CO_2 flux and microbial biomass in natural and managed ecosystems in southern Wisconsin. *Soil Biology and Biochemistry* **30**(12), 1501–1509.

Walia V., Lin S.J., Fu C.C., Yang T.F., Hong W.L., Wen K.L. *et al.* 2010. Soil-gas monitoring: a tool for fault delineation studies along Hsinhua Fault (Taiwan), Southern Taiwan. *Applied Geochemistry* **25**, 602–607. doi: 10.1016/j.apgeochem.2010.01.017

Wannamaker P.E., Caldwell T.G., Doerner W.M. and Jiracek G.R. 2004. Fault zone fluids and seismicity in compressional and extensional environments inferred from electrical conductivity: the New Zealand Southern Alps. *Earth Planets Space* **56**, 1171–1176.

Yang T.F., Chou C.Y., Chen C.H., Chyi L.L. and Jiang J.H. 2003. Exhalation of radon and its carrier gases in SW Taiwan. *Radiation Measurements* **36**, 425–429. doi:10.1016/S1350-4487(03)00164-1.

Yang T.F., Walia V., Chyi L.L., Fu C.C. *et al*. 2005. Variations of soil radon and thoron concentrations in a fault zone and prospective earthquakes in SW Taiwan. *Radiation Measurements* **40**, 496–502. doi:10.1016/j.radmeas.2005.05.017